공학석사 학위논문

Systematic Studies on the Substitution of Ge^{4+} by its Homologue Sn^{4+} in $Li_{1.5}Al_{0.5}Ge_{1.5}(PO_4)_3$ Solid Electrolyte

$Li_{1.5}Al_{0.5}Ge_{1.5}(PO_4)_3$ 고체전해질에서 Ge^{4+} 의 동족체인 Sn^{4+}의 치환에 관한 체계적인 연구

2018 년 8 월

서울대학교 대학원
재료공학부
Misael Ali Mita

Systematic Studies on the Substitution of Ge^{4+} by its Homologue Sn^{4+} in $Li_{1.5}Al_{0.5}Ge_{1.5}(PO_4)_{--3}$ Solid Electrolyte

지도교수 신광선

이 논문을 공학석사학위논문으로 제출함

2018 년 8 월

서울대학교 대학원

재료공학부(학과 및 전공)

Misael Ali Mita(논문 작성자)

Misael Ali Mita 의 석사학위논문을 인준함

2018 년 8 월

위 원 장 강 기 석 (인)

부 위 원 장 신 광 선 (인)

위 원 최 인 석 (인)

Abstract

Along with many technologies developed to store energy for electric vehicles and portable electronic devices, solid state batteries are getting serious attention due to advantages such as high energy density and solution to the safety issues. A solid-state battery is a battery that has both solid electrodes and solid electrolytes. Replacing the organic liquid electrolyte with a solid state ionic conductor would improve safety and the direct-series-stacking of cells can result in a high energy density for the battery. Until now many oxides-based super-ionic materials such as LISICON, NASICON, Pervovskite and Garnet type have been investigated as electrolyte. However, interestingly most of them include expensive elements and this can be a barrier for further scaling up.

In this thesis, the focus has been positioned in the $Li_{1.5}Al_{0.5}Ge_{1.5}(PO_4)_3$ NASICON electrolyte. Main reasons were high ionic conductivity, wide electrochemical window, easy synthesis and good stability with the environment. However, although this electrolyte has many attractive advantages, it contains the expensive cation Ge^{4+}. For this reason, its inexpensive homologue Sn^{4+} was considered for substitution, considering its larger ionic radii which can open the pathways for the lithium ion mobility in the structure. Moreover, cost analysis indicated that Sn^{4+} was 59 times cheaper than Ge^{4+} which can result in an additional important advantage for the tin-bearing ionic conductors. First, a systematic substitution was carried out in the

system $Li_{1.5}Al_{0.5}Ge_{1.5-y}Sn_y(PO_4)_3$ with y = 0.00, y = 0.25, y = 0.50, y = 0.75 and y = 1.00 by conventional solid state reaction. X-ray diffraction showed successful substitution until level y = 1.00. It was not possible to fully substitute Ge^{4+} due to impurity problems. Additionally, from the structural information extracted from the X-ray diffraction pattern, it was seen an increase in the lattice parameters for all tin containing NASICON materials. Furthermore, dense pellets were sintered by classical Spark Plasma Sintering (SPS) and annealing steps were carried out in order to remove graphite contamination and recover the white coloration of all the pellets. The NASICON pellets were characterized by Electrochemical Impedance Spectroscopy (EIS) and the analysis of the electrical data showed that tin addition produced slightly lower ionic conductivity at various concentration levels. In order to elucidate the decrease in the ionic conductivity, Raman spectra were recorded. The results showed that the decrease in ionic conductivity was due to the local disorder in the MO_6 units group in the NASICON crystal structure which resulted in a distortion of the bottleneck regions reducing the charge carrier mobility. Moreover, DC-polarization was carried out and the results showed that synthesized materials had lower electronic conductivity compared to the pristine material. This is a desirable property for LIB in order to avoid the self-discharge. Finally, as a contribution from this work it was found three new solid electrolytes in the system $Li_{1.5}Al_{0.5}Ge_{1.5-y}Sn_y(PO_4)_3$, among them $Li_{1.5}Al_{0.5}Ge_{0.50}Sn_{1.00}(PO_4)_3$ has the higher substitution level and ionic conductivity comparable to the well-known

$Li_{1.5}Al_{0.5}Ge_{1.5}(PO_4)_3$, this expands more the research on inexpensive oxide solid electrolytes feasible for applications.

Keywords: NASICON Solid Electrolyte, Spark Plasma Sintering, Electrochemical Impedance Spectroscopy, Raman Spectroscopy, Lithium Batteries

Student Number: 2016 – 22079

Table of Contents

Abstract **1**

Table of Contents **4**

List of Figures **6**

List of Tables **8**

Chapter 1. Introduction **9**

1.1 Introduction 9

1.2 Spark Plasma Sintering 12

1.3 Impedance Spectroscopy 13

1.4 DC polarization 16

Chapter 2. Experimental Procedure **18**

2.1 Synthesis of $Li_{1.5}Al_{0.5}Ge_{1.5}(PO_4)_3$ and $Li_{1.5}Al_{0.5}Ge_{1.5-y}Sn_y(PO_4)_3$ 18

2.2 X-ray diffraction 19

2.3 SEM observations 20

2.4 Spark Plasma Sintering 20

2.5 Annealing of samples 21

2.6 Electrochemical Impedance Spectroscopy (EIS) 21

2.6.1 Sample preparation 21

2.6.2 AC impedance measurements 22

2.6.3 DC polarization 23

2.7 Raman Spectroscopy 23

Chapter 3. Results and discussion 24

3.1 Structural analysis 24

3.2 Powder morphology 29

3.3 Spark Plasma Sintering (SPS) of NASICON powders and annealing steps 30

3.4 Ionic conductivity 33

3.5 Structural distortion 38

3.5.1 Modification of the bottleneck regions as a function of PO_4 distortion 41

3.6 Electronic conductivity 42

Chapter 4. Conclusion 45

References 46

List of Figures

Figure 1.1 Scheme of the SPS unit.....13

Figure 1.2 Impedance data for $Ca_{12}A1_{14}0_{33}$, presented in- the complex impedance plane format, Z'' vs Z' where Z* = Z'-j Z'', j =−1, ω = angular frequency 2πf. Selected frequency points, in Hz are marked. The equivalent circuit used to interpret the data is shown. It represents a series combination of crystal and grain boundary impedances.....15

Figure 2.1 Schematic set up consisting of Au coated solid electrolyte assembled into a coin cell using stainless steel as a current collector for EIS studies.....22

Figure 3.1 X-ray diffraction (XRD) patterns of synthesized NASICON powders according to the substitution condition. Substitution element is described with "y" in $Li_{1.5}Al_{0.5}Ge_{1.5-y}Sn_y(PO_4)_3$. 25

Figure 3.2 Lattice parameter as a function of the Sn substitution in the system $Li_{1.5}Al_{0.5}Ge_{1.5-y}Sn_y(PO_4)_3$. The determined values follow the linear trend of Vegard's law.....28

Figure 3.3 Images of NASICON powders obtained by SEM: a) y = 0.00, b) y = 0.25, c) y = 0.50, c) y = 0.75 and d) y = 1.00.....29

Figure 3.4 (a - c) Images of annealed pellet at a) 600, b) 700 and c) 800 °C where the sample belongs to the substitution condition y = 0.50 in $Li_{1.5}Al_{0.5}Ge_{1.5-y}Sn_y(PO_4)_3$. **(d - h)** Complete set of pellets after the last annealing treatment at 800 °C according

to the substitution condition. Order of the images starts from d) for y = 0.00 increasing until h) for y = 1.00. 31

Figure 3.5 X-ray diffraction (XRD) patterns of the sintered pellets in the system $Li_{1.5}Al_{0.5}Ge_{1.5-y}Sn_y(PO_4)_3$ after the last annealing treatment at 800 °C. 32

Figure 3.6 a) Complex impedance spectra recorded for system $Li_{1.5}Al_{0.5}Ge_{1.5-y}Sn_y(PO_4)_3$ at 25 °C. **b)** Each fit data was modeled with an equivalent circuit involving resistances (R_1: External resistances, R_2: Bulk resistance, R_3: Grain boundary resistance and R_4: Resistance from electrode polarization) and constant phase elements (Q). 34

Figure 3.7 Arrhenius plots of total conductivities obtained from the complex impedance plots 35

Figure 3.8 Activation energy (E_a) and total ionic as a function substitution condition of $Li_{1.5}Al_{0.5}Ge_{1.5-y}Sn_y(PO_4)_3$ at 25 °C. 36

Figure 3.9 a) Raman spectrum of $Li_{1.5}Al_{0.5}Ge_{1.5-y}Sn_y(PO_4)_3$ in the frequency region of 150 to 1300 cm^{-1}. **b)** NASICON crystal structure where PO4 and MO6 structural groups are highlighted. 39

Figure 3.10 Raman spectra in the range of 850 – 1300 cm^{-1} for studying stretching modes ν_1 and ν_3. 40

Figure 3.11 MO_6/PO_4 rotation and/or distortion. 42

Figure 3.12 a) Experimental result of the electronic conductivity measurement vis DC-polarization method. **b)** Electronic conductivity as a function substitution condition of $Li_{1.5}Al_{0.5}Ge_{1.5-y}Sn_y(PO_4)_3$ at 25 °C. 43

List of Tables

Table 2.1 Prepared powders in the system $Li_{1.5}Al_{0.5}Ge_{1.5-y}Sn_y(PO_4)_3$.....19

Table 2.2 Annealing conditions for recovering pristine physical and chemical characteristics of samples after classical SPS 21

Table 3.1 Unit cell information for NASICON materials obtained by full pattern matching in the space group $R\bar{3}c$ (Rhombohedral). 27

Table 3.2 Sintering parameters and relative densities after classical SPS and after annealing at 800 °C. 30

Table 3.3 Summary total ionic conductivities, electronic conductivities, activation energy, ionic transference number and relative density with composition $Li_{1.5}Al_{0.5}Ge_{1.5-y}Sn_y(PO_4)_3$. 44

Chapter 1. Introduction

1.1 Introduction

Recent observations confirm that the world's oil and natural gas supplies are running out too fast and, soon they will fall below the level required to meet international demands. It appears critical to consider ecological electricity generation systems (photovoltaic, windmill, geothermic energy…) and to associate them with energy storage systems. Rechargeable batteries are the oldest form of electricity storage and the most widely used. Despite important progress over the last twenty years, the improvements of conventional liquid/gel based Li-ion batteries are slowing down and breakthroughs are needed. In regards to tomorrow's energy needs, it is necessary to develop energy storage systems with high energy densities, long life, low cost, little or no maintenance and a high degree of safety.

All-solid-state batteries may meet these requirements because of their low loss of capacity as a function of time, their thermal stability, their absence of leakage and pollution (solvent free). However, the energy densities of such technology remain restricted, mainly due to limitations in their development. Since 1982, all-solid-state thin film batteries have always been under significant improvements but their energy densities are still too low for large applications[1].

A solid-state battery is a battery that has both solid electrodes and solid electrolytes. Replacing the organic liquid electrolytes with a solid state ionic conductor would

improve device safety tremendously and remove one of the few remaining barriers to even wider scale use of Li-ion technology.

Safety issues are of immense concern in developing advanced energy storage technologies, especially for Li-ion batteries. Commercial Li-ion batteries contain flammable organic liquid electrolyte that poses major technical challenges; most recent major incidents of Li-ion battery fires were caused by the ignition of the electrolyte. Inorganic solid-state Li-ion conductors also benefit from many other advantages such as superior electrochemical, mechanical and thermal stability, absence of leakage, and the possibility of battery miniaturization [2].

Li-ion solid-state conductors require high ionic conductivity at room temperature and low activation energy (E_a) for use over a broad range of operating temperatures. In addition, other properties such as electrochemical stability against the anode and cathode, and environmental stability are preferred as they reduce the complexity of the battery[2].

Inorganic solid electrolytes can be sulfide-based or oxide-based. Among sulfide-based solid electrolytes (SBSEs), $Li_{10}GeP_2S_{12}$ (LGPS) shows the highest ionic conductivity, ~1.2×10^{-2} $S \cdot cm^{-1}$ at room temperature; this exceeds the ionic conductivity of conventional liquid electrolyte. However, LGPS suffers from strong reactivity with air and moisture which can lead to an expensive synthesis and other SBSEs suffer from strong reactivity with air and Li metal. Oxide-based solid electrolytes (OBSEs) have been actively developed to achieve high ionic

conductivity; they also have high stability with Li metal or air. However, the ionic conductivity of OBSEs is not high enough because of very low grain boundary conductivity. Many efforts have been focused on improving grain boundary conductivity of OBSEs. The main idea for these efforts is to minimize the effect of grain boundaries on ionic conductivity[3]. Methods to accomplish this minimization include Spark Plasma Sintering (SPS) to increase OBSE density.

Among OBSEs, $Li_{1.5}Al_{0.5}Ge_{1.5}(PO_4)_3$ (LAGP) has several advantages over other electrolytes such as $Li_{1+x}Al_xTi_{2-x}(PO_4)_3$ (LATP) or $Li_7La_3Zr_2O_{12}$ (LLZO). Although LAGP and LATP have the same NASICON-type structure, LAGP has a wide electrochemical window whereas LATP has a narrow one because LATP reacts with Li metal at ~2.4 V (vs. Li/Li^+) due to the redox reaction of Ti^{4+}. Compared to garnet-type solid electrolytes such as LLZO, LAGP can be easily synthesized without any phase transition during synthesis. LAGP has the expensive element germanium which according to USGS showed costs in last years around 1150 $/Kg. This cost is tremendously high and can be a big issue for the applications of this materials in the industry. On the other hand, according to the London Metal Exchange tin showed prices around 19.5$/Kg in 2018. Comparing these two elements, tin is 59 times cheaper which make it an attractive element for replacing germanium in the system LAGP.

Moreover, in the next sections it is going to be described briefly the Spark Plasma Sintering process to densify solid electrolytes and methods to characterize the electrical properties.

1.2 Spark Plasma Sintering

The Spark Plasma Sintering (SPS) technique (also called Pulsed Electric Current Sintering (PECS) or Field Assisted Sintering Technology (FAST)) is a pressure assisted sintering method that uses pulsed high DC current along with uniaxial pressure to consolidate oxide solid electrolytes. It has been successfully used for the sintering of nanostructured materials, transparent materials, polymers, composites, etc. Even materials which are considered to be difficult to sinter can be sintered to full density using SPS. Economic and technological benefits of SPS compared to conventional sintering methods can be summarized as: i) faster heating/cooling rates, ii) lower sintering temperature and iii) shorter holding time. Compared with the conventional sintering methods, SPS allow a rapid densification (typically a few minutes) at lower temperatures and allow obtaining higher density, smaller grain size, cleaner grain boundaries, and other attractive properties[4].

A SPS unit is schematically shown in Figure 1.1. It consists of a uniaxial pressure device, where the water-cooled punches also serve as electrodes, a watercooled chamber that can be evacuated, a pulsed DC generator and a computer-based process controller which also records the shrinkage, temperature, pressure, average voltage and current during the process. Powders are placed on a die (typically graphite) and

heating is carried out by passing a current through the die and the sample (if it is conducting) while a pressure is applied on the powder[4].

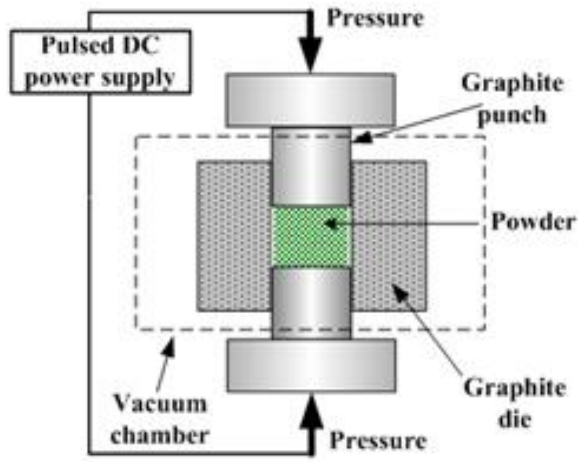

Figure 1.1 Scheme of the SPS unit

1.3 Impedance Spectroscopy

An alternative technique for measuring electrical properties of solid electrolytes is impedance spectroscopy. In this, AC impedance measurements are made over a wide range of frequencies and the different regions of the material are characterized according to their electrical relaxation times or time constants. Impedance spectroscopy is relatively easy to use and is applicable to a wide variety of materials and problems. It has undergone major developments recently with the availability of automatic equipment capable of spanning many decades of frequency in a single sweep. Different regions of a ceramic sample are characterized by a resistance and a

capacitance, usually placed in parallel. The characteristic relaxation time or time constant, τ, of each 'parallel RC element' is given by the product of R and C (Equation 1.1).

$$\tau = RC \qquad 1.1$$

$$\omega_{max} = RC = 1 \qquad 1.2$$

In the frequency domain, RC elements are separable due to the relation shown in Equation 1.2 which holds at the frequency of maximum loss, ω_{max}, in the impedance spectrum. From the impedance spectrum, it is therefore usually possible to identify different RC elements and assign them to appropriate regions of the sample. The values of the individual R and C components may then be quantified. Let us now see some practical example of data and interpretation.

A common type of impedance spectrum for electroceramics shows the presence of two distinct features attributable to intragrain, or bulk and intergrain, or grain boundary regions. A typical case is shown in Figure 1.2 a for the oxide ion conductor $Ca_{12}A1_{14}0_{33}$.

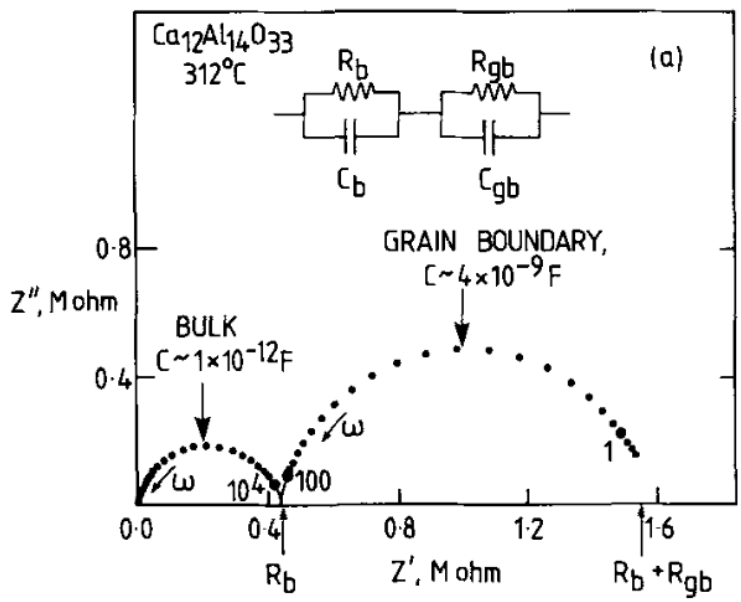

Figure 1.2 Impedance data for $Ca_{12}A1_{14}0_{33}$, presented in- the complex impedance plane format, Z'' vs Z' where Z* = Z'-j Z'', j =$\sqrt{-1}$, ω = angular frequency $2\pi f$. Selected frequency points, in Hz are marked. The equivalent circuit used to interpret the data is shown. It represents a series combination of crystal and grain boundary impedances.

Impedance data are presented in the form of imaginary, Z" (capacitive) against real, Z' (resistive) impedances. Each parallel RC element (two in Figure 1.2) gives rise to a semicircle (ideally) from which the component R and C values may be extracted. R values are obtained from the intercepts on the Z' axis, as shown; C values are obtained by applying Equation 1.2 to the frequency at the maximum of each semicircle. In this particular case, the two capacitance values are determined to be

around $1x10^{-12}$ F and $4x10^{-9}$ F and the corresponding resistances 0.45 Mohm and 1.15 Mohm[5].

1.4 DC polarization

Since the ionic/superionic solids obey the Ohm's law pretty well i.e. the instant initial total current varies directly as a function of the potential (V) applied across the specimen when V is kept below the decomposition potential of the sample material. Hence, dc polarization method can be considered to be one of the appropriate technique to determine some basic ionic parameters which in turn would help us to explain the ion transport behavior in these solids.

The transference number gives a quantitative information of the extent of ionic and electronic (electrons and holes) contribution to the total conductivity (σ_T). Since, $\sigma_T = \sigma_{ion} + \sigma_{e.h}$, the ionic/electronic transference number can be defined as:

$$t_{ion} = \frac{\sigma_{ion}}{\sigma_T} = \frac{I_{ion}}{I_T} \qquad 1.3$$

$$t_{e,h} = \frac{\sigma_{e,h}}{\sigma_T} = \frac{I_{e,h}}{I_T} \qquad 1.4$$

Where $\sigma_{ion}/\sigma_{e,h}$ and $I_{ion}/I_{e,h}$ are the conductivity and current contribution due to ionic/(electrons/holes) respectively. The total current is expressed by the equation: $I_T = nqv_dA$, where q is the charge on the ion and A is the area of the cross section. The ionic transference number can be determined accurately by Wagner's method. This is a most convenient and widely used method suggested to measure the

ionic/electronic transference number in number of solid electrolyte systems. For this method a sample is sandwiched is sandwiched between two blocking electrodes (stainless steel) and a constant DC potential (V~0.5V) is applied across the sample with polarity and current in the circuit is monitored as a function of time with the help of a recorder. In a typical current versus time plot the total current approaches to zero, however if the solid is a mixed ionic/electronic system the total current I_T levels off at some non-zero value. The final residual current ($I_{e,h}$) is due to the moving electrons/holes in the system[6].

In the present work, a systematic substitution of the expensive element Ge^{4+} by its homologue Sn^{4+} in $Li_{1.5}Al_{0.5}Ge_{1.5}(PO_4)_3$ solid electrolyte was carried out. The study is based on the rationale that larger Sn^{4+} (0.69A) will open the bottleneck points in the crystal structure and promote enhanced lithium ion mobility. Five different materials were reported in the system $Li_{1.5}Al_{0.5}Ge_{1.5-y}Sn_y(PO_4)_3$ with y = 0.00, 0.25, 0.50, 0.75 and 1.00. Moreover, Spark Plasma Sintering process was used to densify the NASICON powders, X-ray diffraction (XRD) was used to study the structural aspects, Raman spectroscopy to study the local order of PO_4 groups in the anionic backbone of the structure and Electrochemical Impendence Spectroscopy to study the ionic and electrical behavior of the specimens.

Chapter 2. Experimental Procedure

2.1 Synthesis of $Li_{1.5}Al_{0.5}Ge_{1.5}(PO_4)_3$ and $Li_{1.5}Al_{0.5}Ge_{1.5-y}Sn_y(PO_4)_3$

NASICON solid electrolyte LAGP ($Li_{1.5}Al_{0.5}Ge_{1.5}(PO_4)_3$ was synthesized by the conventional solid-state reaction. Stoichiometric amounts of Li_2CO_3 (99%), Al_2O_3, GeO_2 (99.99%) and $(NH_4)H_2PO_4$ (98%) were purchased from Sigma-Aldrich and used as received [7]. The mixture was thoroughly dispersed in isopropyl alcohol by using a planetary ball milling apparatus (Pulverisette 5, Fritsch) and dried at 35 °C for 24 h to evaporate the solvent. The powder mixture was heated to 700 °C at a heating rate of 5 °$Cmin^{-1}$ in a tube furnace and held at that temperature for 2 h to release any volatile compounds. The powder was pulverized by ball milling at 300 rpm for 5 h followed by heating to 850 ºC with a heating rate of 5 °$Cmin^{-1}$ and calcined at the same temperature for 12 h in argon atmosphere[8]. The heated sample was pulverized again by ball milling at 300 rpm for 16 h.

Powders with different level of substitution in the system $Li_{1.5}Al_{0.5}Ge_{1.5-y}Sn_y(PO_4)_3$ were prepared using the same precursors as mentioned above and SnO_2 (99.9%) was used as a tin source. The chemical formula of all the materials is listed in Table 2.1.

Table 2.1 Prepared powders in the system $Li_{1.5}Al_{0.5}Ge_{1.5-y}Sn_y(PO_4)_3$

Material	y
$Li_{1.5}Al_{0.5}Ge_{1.5}(PO_4)_3$	0.00
$Li_{1.5}Al_{0.5}Ge_{1.25}Sn_{0.25}(PO_4)_3$	0.25
$Li_{1.5}Al_{0.5}Ge_{1.00}Sn_{0.50}(PO_4)_3$	0.50
$Li_{1.5}Al_{0.5}Ge_{0.75}Sn_{0.75}(PO_4)_3$	0.75
$Li_{1.5}Al_{0.5}Ge_{0.50}Sn_{1.00}(PO_4)_3$	1.00
$Li_{1.5}Al_{0.5}Ge_{0.25}Sn_{1.25}(PO_4)_3$	1.25
$Li_{1.5}Al_{0.5}Sn_{1.50}(PO_4)_3$	1.50

When "y" was 0.25 and 0.50 it was used exactly same method as described above to synthesize the new powders. However, when "y" was more than 0.75 two additional heating steps at 180 and 200 °C at a heating rate of 1.5 °Cmin^{-1} were needed before 700 °C treatment. These steps were used to avoid melting of some precursors and further loss of material during the process. It is speculated that some eutectic point was formed by the addition of tin oxide in the mentioned amounts.

2.2 X-ray diffraction

X-ray diffraction (XRD) patterns of $Li_{1.5}Al_{0.5}Ge_{1.5-y}Sn_y(PO_4)_3$ powdered samples were recorded with CuK_α radiation (λ = 1.5418 Å) using Bruker New D8 Advance diffractometer operated at 40 kV and 40 mA in the 2θ range of 10 – 45° with a step size of 0.02 and collection time of 3 s. Full pattern matching method of the data was

carried out using Fullprof software to extract lattice parameters using $LiGe_2(PO_4)_3$ JCPDS File Card No. 80-1922.

2.3 SEM observations

The morphology and particle size distribution of all prepared powders were visualized using MERLIN Compact FE-SEM using an acceleration voltage of 15 kV in the secondary electron mode. Samples were coated with Pt and a 7k times magnification were used for the images coming from randomly chosen location. Due to overlap between particles, it was considered more reliable to identify and measure the particle diameters using the image processing program ImageJ.

2.4 Spark Plasma Sintering

Dense pellets have been prepared using classical SPS. The powders were loaded in a cylindrical graphite die with 12 mm of inner diameter and enclosed by graphite sheets. Uniaxial load was gently increased until getting a pressure of 90 Mpa in a vacuum state and an electric current ranging around 800 A and voltage of 3.2 V was applied. The heating rate was 100 °Cmin^{-1}, the sintering temperature 750 °C and the holding time of 5 min. The temperature was monitored by a thermocouple inserted into the graphite die. After holding for a predetermined time, the electric current was stopped and the graphite setup was cooled inside the chamber until reaching 100 °C, finally, the pressure was released. The graphite sheets adhered to the pellets were removed by polishing in sandpaper and the density of the samples was determined from the weight and physical dimensions. From the other side, the theoretical

densities of all samples were calculated from results obtained from full pattern matching method. Combining these results, the relative density of sintered pellets was quantified.

2.5 Annealing of samples

Different annealing steps in air and polishing were carried out in order to remove the graphite contamination and recover the white coloration of all the samples. The experimental conditions are presented in Table 2.2.

Table 2.2 Annealing conditions for recovering pristine physical and chemical characteristics of samples after classical SPS

Annealing Step	Heating Rate (°C/min)	Temperature (°C)	Holding Time (h)
First	1	600	3
Second	1.5	700	3
Third	1.5	800	3

To confirm the presence of the NASICON phase X-ray diffraction analysis was made. Moreover, the relative density after the third thermal treatment was calculated with the same method described above.

2.6 Electrochemical Impedance Spectroscopy (EIS)

2.6.1 Sample preparation

All pellets obtained after annealing steps were carefully polished through sandpapers number 600, 800, 1000, 1500, 2000 and lapping film of 3 μm until obtaining a perfect

mirror surface on both faces. A Coater was used to deposit pure gold onto each active area of the pellets and subsequently they were dried at 200 °C for 4 h in argon atmosphere inside a glovebox. After this moment the samples weren't exposed to the environment anymore to prevent side reactions on the surface. Au coated specimens were then assembled into a coin cell using stainless steel as a current collector in a glove box as illustrated in Figure 2.1.

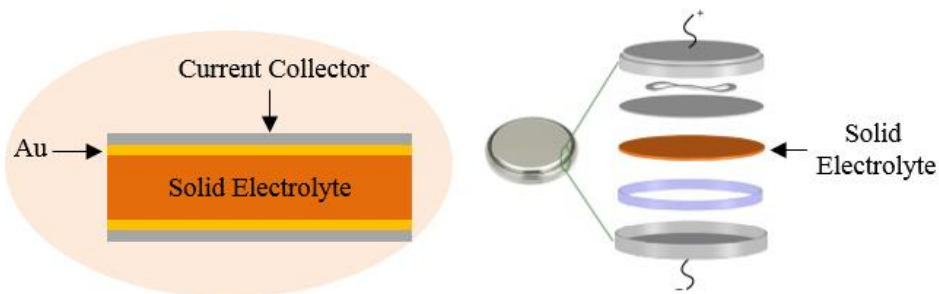

Figure 2.1 Schematic set up consisting of Au coated solid electrolyte assembled into a coin cell using stainless steel as a current collector for EIS studies.

2.6.2 AC impedance measurements

AC impedance measurements were carried using a Solartron impedance analyzer (model HF1225) over the frequency range between 10 Hz and 3 MHz with a voltage amplitude of 10 mV at different temperatures. Each sample was allowed to equilibrate for 15 min at the required temperature before measurements. The data was analyzed by using EC-Lab® software and ionic conductivity values were obtained from:

$$\sigma = \frac{d}{AR} \qquad 2.1$$

where d is the sample thickness, A is the area of the electrodes and R is the sample resistance. The activation energy was calculated from the temperature dependence of conductivity.

2.6.3 DC polarization

DC polarization measurements were undertaken at 25 °C to obtain the electronic conductivity using the same electrochemical work station and cells used previous experiment. The potential applied was 1 V and time was 60 min.

2.7 Raman Spectroscopy

Raman spectra were recorded to study the structural changes of the synthesized electrolytes in the range of 150−1300 cm^{-1}. HORIBA LabRAM HV Evolution system equipped with a 532-nm laser was used and the Raman shift was calibrated using a silicon standard.

Chapter 3. Results and discussion

3.1 Structural analysis

The NASICON $LiM_2^{4+}(PO_4)_3$ (M = Ge, Ti, Hf, Sr, etc) has a rhombohedral structure with space group $R\bar{3}c$ where the structure has a unit cell ($Li_6M_{12}P_{18}O_{72}$) containing 6 formula units ($LiM_2(PO_4)_3$). This framework is mainly constructed by a covalent skeleton $[M_2P_3O_{12}]^-$ with MO_6 octahedra and PO_4 tetrahedra in which each MO_6 octahedra shares its six corners with the tetrahedra, and each tetrahedral shares its four corners with the octahedral. Trivalent and divalent cations are usually used as a partial substitution of M^{4+} to increase the amount of Li ions and hence to enhance ionic conductivity [9]. As it is advised by Winand et al. [10] the adequate ionic radius difference between two cations is $\Delta r = 0.1$ Å as an upper limit in order to have solid solution formation. Al^{3+} (0.535 Å) and Ge^{4+} (0.53 Å) ionic radius difference is 0.005 Å therefore is expected they intermix. On the other hand, Sn^{4+} (0.69 Å) and Ge^{4+} has a difference of 0.16 Å which would lead to an unlikely scenario. Nevertheless, in previous studies, NASICON solid solution formation was synthesized despite exceeding the mentioned upper limit[11].

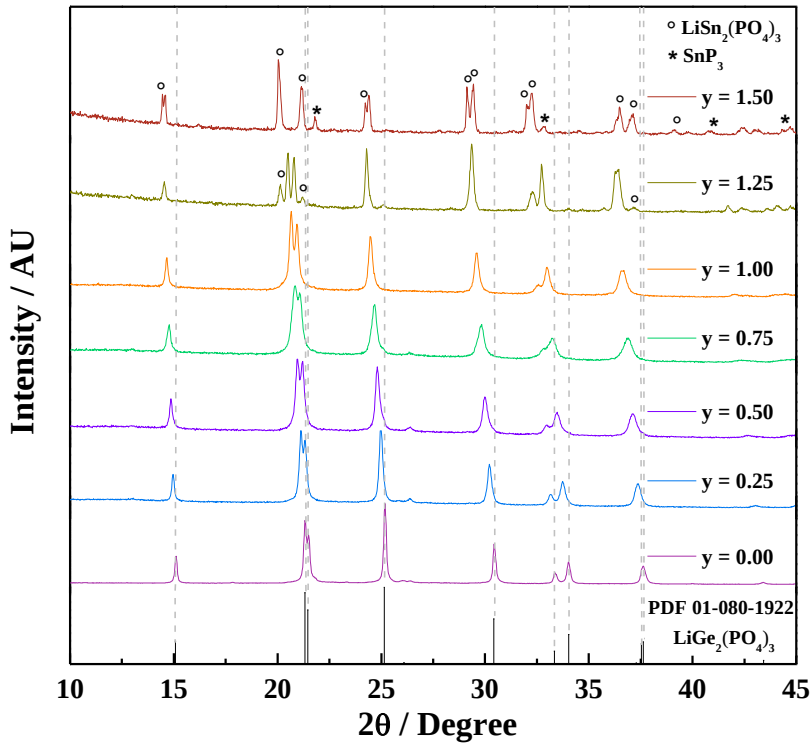

Figure 3.1 X-ray diffraction (XRD) patterns of synthesized NASICON powders according to the substitution condition. Substitution element is described with "y" in $Li_{1.5}Al_{0.5}Ge_{1.5-y}Sn_y(PO_4)_3$.

Figure 3.1 shows the XRD patterns of the $Li_{1.5}Al_{0.5}Ge_{1.5-y}Sn_y(PO_4)_3$ powders after 12 h of thermal treatment at 850 °C. For the pristine material with y = 0.00, the rhombohedral NASICON phase was obtained in agreement with previous reports and it can be indexed based on $LiGe_2(PO_4)_3$ (JCPDS File Card No. 80-1922) [3, 7]. This material exhibited sharp peaks confirming the solid solution formation with good long range-range crystal ordering. With y = 0.25 and y = 0.50, the XRD

patterns showed the formation of a single phase material with NASICON structure and most importantly the data clearly confirmed the successful substitution of germanium by tin. Both materials exhibited fairly sharp peaks confirming NASICON solid solution formation with good long-range crystal ordering. With y = 0.75 and 1.00, the XRD data confirmed the dominant formation of single phase materials with the NASICON structure. In these cases, however, the diffraction patterns showed slight peak broadening which can be an evidence of the disruption of the long-range order of the crystal. This might be due to an insufficient thermal treatment for favoring the migration of higher quantities of large Sn^{4+} ions as Brian et al. reported[11, 12]. Moreover, from substitution level y = 0.25 to y = 1.00, it was observed a gradual shift of all the Bragg peaks to the lower 2θ value indicating the increase of the lattice parameters in the NASICON structure.

With y = 1.25 and y = 1.50, it was not possible to synthesize the pure studied phase. At y = 1.25 it was seen peaks corresponding to the NASICON phase but also the monoclinic $LiSn_2(PO_4)_3$ phase (JCPDS File Card No. 49-1175) began to appear[13]. With complete substitution (y = 1.50) it was seen the dominant formation of the monoclinic phase, additionally few peaks coming from the NASICON phase were observed coexisting with a small fraction of SnP_3. These two materials need further investigation.

In summary, the diffraction patterns illustrated in Figure 3.1 showed the NASICON phase in most cases with gradual evolution in the characteristics of the peaks. Five

materials were successfully synthesized and will be considered for further studies. Moreover, it is worthy to highlight that the materials $Li_{1.5}Al_{0.5}Ge_{1.25}Sn_{0.25}(PO_4)_3$, $Li_{1.5}Al_{0.5}Ge_{1.00}Sn_{0.50}(PO_4)_3$ and $Li_{1.5}Al_{0.5}Ge_{0.50}Sn_{1.00}(PO_4)_3$ were synthesized for the first time.

Table 3.1 summarizes unit cell information obtained by full pattern matching in the space group $R\bar{3}c$ by using FullProf program. For y = 0.00, the lattice parameters are in good agreement with previous reports[14, 15]. On the other hand, as soon as tin was incorporated in the structure and systematically increased, the lattice parameters increased as well. This fact was expected and previous studies indicated that the incorporation of tin increases spacing within columns of MO_6 units as well as between them, consequently suggesting an opening of conduction channels [12].

Table 3.1 Unit cell information for NASICON materials obtained by full pattern matching in the space group $R\bar{3}c$ (Rhombohedral).

$Li_{1.5}Al_{0.5}Ge_{1.5-y}Sn_y(PO_4)_3$	a (Å)	b (Å)	c (Å)	Unit-cell volume, V($Å^3$)	c/a ratio
y = 0.00	8.27602	8.27602	20.52118	1217.24	2.48
y = 0.25	8.32060	8.32060	20.69565	1240.85	2.49
y = 0.50	8.36387	8.36387	20.88408	1265.20	2.50
y = 0.75	8.41236	8.41236	21.01684	1288.05	2.50
y = 1.00	8.46066	8.46066	21.18879	1313.55	2.50

In Figure 3.2, it is plotted the lattice parameter as a function of tin substitution, it is noticeable to see the linear relationship between them known as Vegard's law which indicates no change in the phase in all cases.

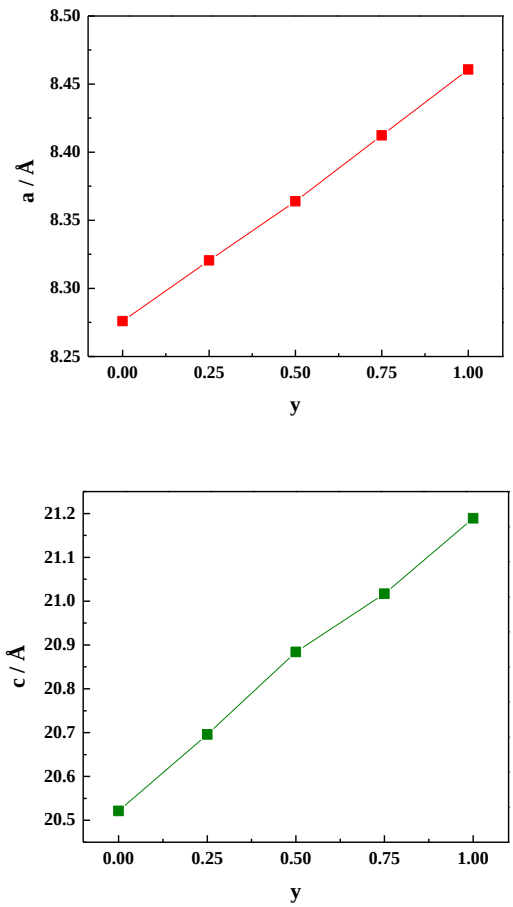

Figure 3.2 Lattice parameter as a function of the Sn substitution in the system $Li_{1.5}Al_{0.5}Ge_{1.5-y}Sn_y(PO_4)_3$. The determined values follow the linear trend of Vegard's law.

3.2 Powder morphology

Scanning electron micrographs of NASICON powders are presented in Figure 3.3. All samples showed particles with round shape without agglomeration and their size ranged as follows: 0.6 – 2.9, 0.5 – 2.7, 0.4 – 2.8, 0.5 – 3.2 and 0.6 – 2.5 μm for materials with level of substitution 0.00, 0.25, 0.50, 0.75 and 1.00 respectively. The results showed similar morphological characteristics for all the samples.

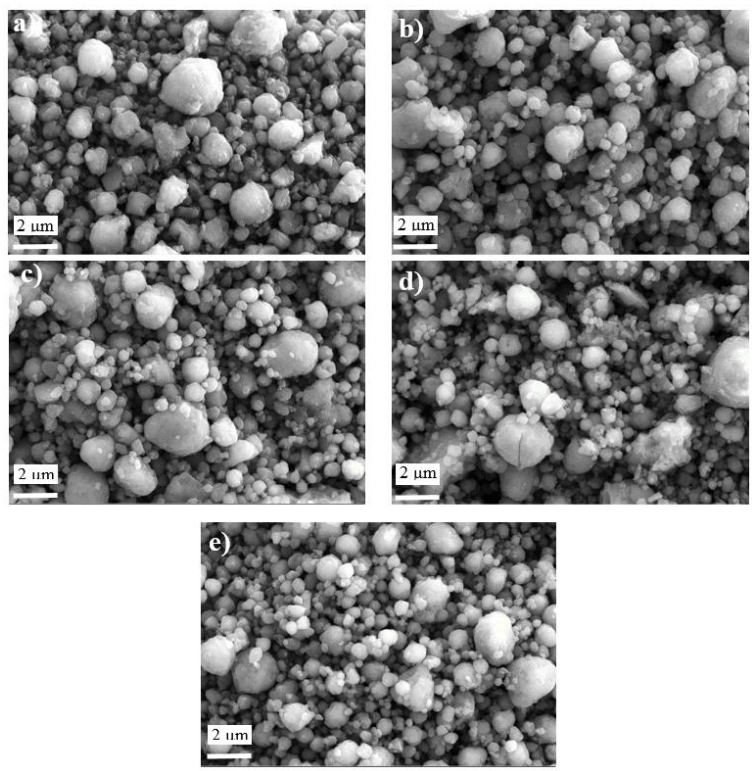

Figure 3.3 Images of NASICON powders obtained by SEM: a) y = 0.00, b) y = 0.25, c) y = 0.50, c) y = 0.75 and d) y = 1.00

3.3 Spark Plasma Sintering (SPS) of NASICON powders and annealing steps

Table 3.2 shows the experimental parameters for the sintering process and also the calculated relative densities. After SPS process, the results showed densification higher than 90% in all cases. On the other hand, after the last annealing step at 800 °C they were over 85%. This condition was higher enough and similar to carry out studies on NASICON solid electrolytes [4, 16, 17].

Table 3.2 Sintering parameters and relative densities after classical SPS and after annealing at 800 °C.

Sample $Li_{1.5}Al_{0.5}Ge_{1.5-y}Sn_y(PO_4)_3$	Heating Rate (°C/min)	Temp. (°C)	Holding Time (min)	Pressure (MPa)	Relative Density after SPS (%)	Relative Density after annealing at 800°C (%)
y = 0.00	100	750	5	90	94.3	90.05
y = 0.25	100	750	5	90	95.3	85.56
y = 0.50	100	750	5	90	95.2	92.33
y = 0.75	100	750	5	90	94.1	91.90
y = 1.00	100	750	5	90	93.5	88.91

Figure 3.4 a-c shows the physical appearance of the pellet with y = 0.50 during the annealing steps in air. At 600 and 700 °C the pellet showed dark-white coloration, on the other side after 800 °C it was completely homogenous and white similar like the initial powder. Others samples with a different level of substitution showed the same behavior. In Figure 3.4 d-h is presented the complete set of pellets after 800 °C. In all cases, they showed white coloration and well defined geometrical shape.

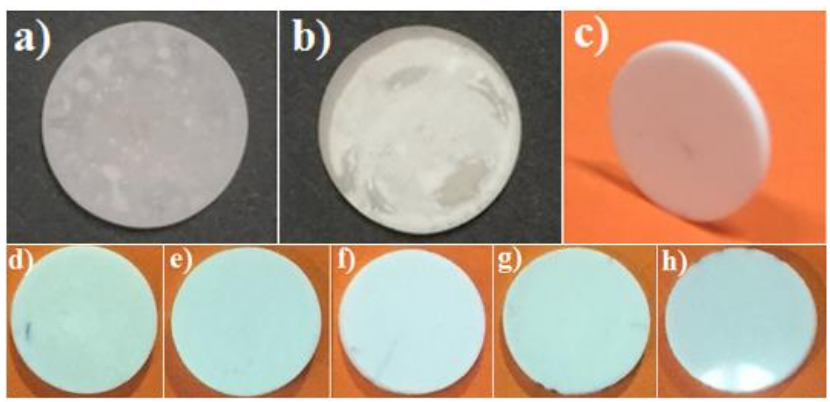

Figure 3.4 (a - c) Images of annealed pellet at a) 600, b) 700 and c) 800 °C where the sample belongs to the substitution condition y = 0.50 in $Li_{1.5}Al_{0.5}Ge_{1.5-y}Sn_y(PO_4)_3$. **(d - h)** Complete set of pellets after the last annealing treatment at 800 °C according to the substitution condition. Order of the images starts from d) for y = 0.00 increasing until h) for y = 1.00.

In Figure 3.5 is presented the XRD patterns of sintered pellets after annealing treatment at 800 °C. In all cases, the data confirmed the presence of the studied rhombohedral NASICON phase.

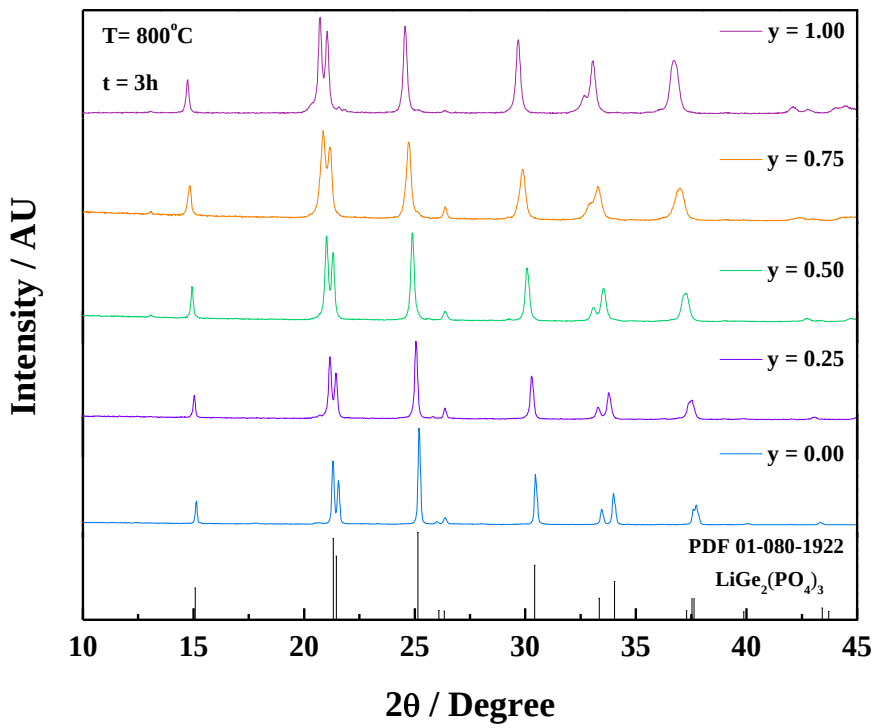

Figure 3.5 X-ray diffraction (XRD) patterns of the sintered pellets in the system $Li_{1.5}Al_{0.5}Ge_{1.5-y}Sn_y(PO_4)_3$ after the last annealing treatment at 800 °C.

3.4 Ionic conductivity

Figure 3.6a shows an example of the typical complex impedance spectra for the system $Li_{1.5}Al_{0.5}Ge_{1.5-y}Sn_y(PO_4)_3$ at 25 °C. At high frequencies, all samples showed a single distorted semicircle representing the total resistance where not clear separation of bulk and grain boundary contributions were observed. On the other hand, at low frequencies a tail related to Warburg-type impedance was seen which reflects the ionic nature of the NASICON materials[18, 19]. Tin containing samples showed slightly higher resistance than the pristine material (detailed analysis will be discussed later). In all cases, the external resistances (R_1) were negligible since the single semicircles suggested their intersection at zero value in the real axes, indicating the reliability of the data.

Moreover, the complex impedance spectra were fitted with the EC-Lab® software to determine the total resistance from which the total ionic conductivity was calculated.

a)

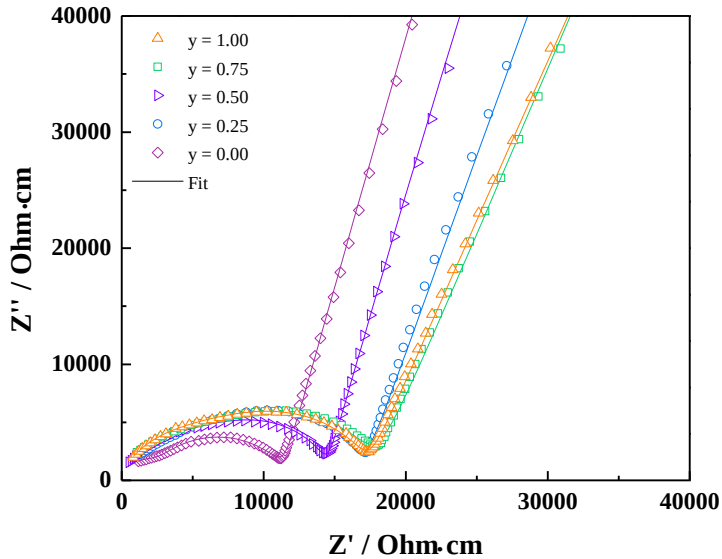

b)

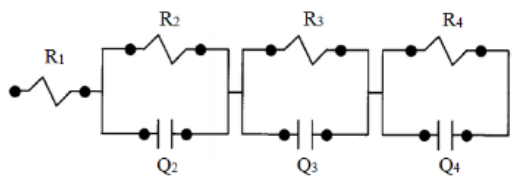

Figure 3.6 a) Complex impedance spectra recorded for system $Li_{1.5}Al_{0.5}Ge_{1.5-y}Sn_y(PO_4)_3$ at 25 °C. **b)** Each fit data was modeled with an equivalent circuit involving resistances (R_1: External resistances, R_2: Bulk resistance, R_3: Grain boundary resistance and R_4: Resistance from electrode polarization) and constant phase elements (Q).

Figure 3.7 shows the temperature dependence of total ionic conductivity for the $Li_{1.5}Al_{0.5}Ge_{1.5-y}Sn_y(PO_4)_3$ system according to the Arrhenius equation.

$$\sigma_T = A\ exp(-\frac{E_a}{kT}) \qquad 3.1$$

where A is the frequency factor, E_a is the activation energy, k is the Boltzmann constant and T is the absolute temperature. All plots showed a linear trend which pointed out that there was no phase change in the temperature range of 25 to 75 ˚C[9]. Furthermore, the lithium ionic conductivities of NASICON materials with a different level of tin substitution were slightly lower than that of the pristine material at all temperatures.

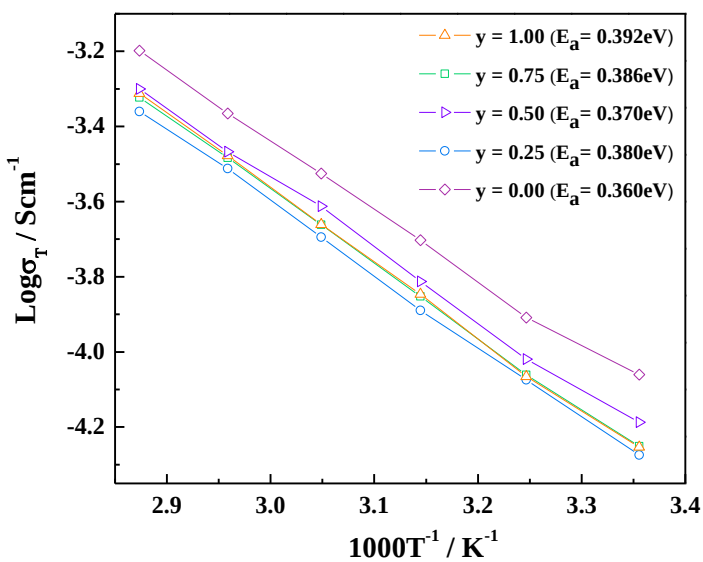

Figure 3.7 Arrhenius plots of total conductivities obtained from the complex impedance plots

Figure 3.8 shows detailed information about the change of the total ion conductivity and the activation energy as a function of substitution condition in $Li_{1.5}Al_{0.5}Ge_{1.5-y}Sn_y(PO_4)_3$ at 25 °C.

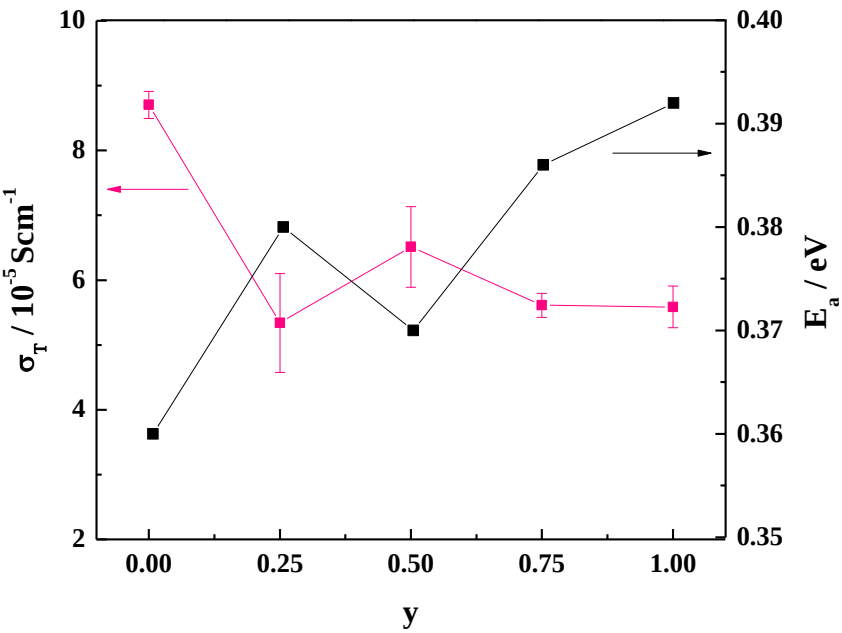

Figure 3.8 Activation energy (E_a) and total ionic as a function substitution condition of $Li_{1.5}Al_{0.5}Ge_{1.5-y}Sn_y(PO_4)_3$ at 25 °C.

For the y = 0.00 sample, the ionic conductivity (8.7×10^{-5} Scm^{-1}) was slightly lower than others reported in the literature. The reason why it was not possible to reach the highest ionic conductivity values, presumably was because the lithium loss during the thermal treatments. Moreover, the activation energy (0.360 eV) was similar to others reports[17, 20]. When Ge^{4+} was substituted by Sn^{+4} in the level of y = 0.25,

the ionic conductivity dropped to the lowest value with higher activation energy compared to y = 0.00. Furthermore, for y = 0.50 sample, the ionic conductivity showed the maximum value for the tin-containing electrolytes with lower activation energy compared to the previous material. Moreover, after this summit, the ionic conductivity decreased and kept almost the same value for the last two electrolytes with a slight increase in the activation energy.

There are few studies about NASICON electrolytes containing Sn^{4+} in the structure and now they are compared to this work. Santagneli et al. reported glassy NASICON samples in the system $Li_{1+x}Al_xSn_yGe_{2-(x+y)}(PO_4)_3$, the total ionic conductivity values were in the order of magnitude 10^{-5}, 10^{-6}, 10^{-7} and 10^{-9} and the activation energies around 0.8 eV[11]. The results in this work showed a group of solid electrolytes in the system $Li_{1.5}Al_{0.5}Ge_{1.5-y}Sn_y(PO_4)_3$ with higher ionic conductivities (~10^{-5} Scm^{-1}) and lower activation energies (~0.3eV) prepared by conventional solid-state reaction. Moreover, Brian et al. synthesized by Pechini-type sol-gel process $LiGeSn(PO_4)_3$ and $Li_{1.5}Al_{0.5}Sn_{0.75}Ge_{0.75}(PO_4)_3$ with bulk ionic conductivities in the order of magnitude 10^{-9} and 10^{-4} respectively. Considering compositional similarities, $LiGeSn(PO_4)_3$ is comparable to y = 1.00 ($Li_{1.5}Al_{0.5}Ge_{0.50}Sn_{1.00}(PO_4)_3$), however, this last material showed considerably higher total ionic conductivity (5.59×10^{-5} Scm^{-1}). This result suggested that the germanium substitution with trivalent ions ($Ge^{+4} \rightarrow Al^{+3} + Li^{+}$) was still an important mechanism to enhance the ionic conductivity of NASICON electrolytes containing Sn^{4+}[21]. On the other hand, the $Li_{1.5}Al_{0.5}Sn_{0.75}Ge_{0.75}(PO_4)_3$ (y = 0.75) material was also studied by Brian et al. and its

ionic conductivity and activation energies values were in good agreement with the values reported in this work.

3.5 Structural distortion

y = 0.75 and y = 1.00 samples showed expected low ionic conductivity values due to the disruption in the crystal ordering according to the XRD data. On the other hand, y = 0.25 and 0.50 samples showed good long range crystal ordering from the XRD. Moreover, the structural information revealed the increase in the lattice parameters suggesting the opening of the bottlenecks. Even though these conditions were favorable for enhancing the ionic conductivity of these two materials, their electrical properties didn't improve. As the literature states, in NASICON materials containing diverse cations with different size, local distortion might affect the ionic conductivity [12, 22]. For this reason, Raman spectroscopy was carried out to study the local order of each material.

In NASICON electrolytes, Raman bands result from the vibration of the PO_4 structural groups[22]. PO_4 tetrahedra connects columns of MO_6 octahedra, sharing oxygen atoms with $M^{4+/3+}$ (Al^{3+}, Ge^{4+}, Sn^{4+}) and lithium ions in the NASICON structure (Figure 3.9 b). Moreover, factor group analysis of these compounds with R-3c space group points out 14 internal modes; 6 stretching modes and 8 bending modes.

a)

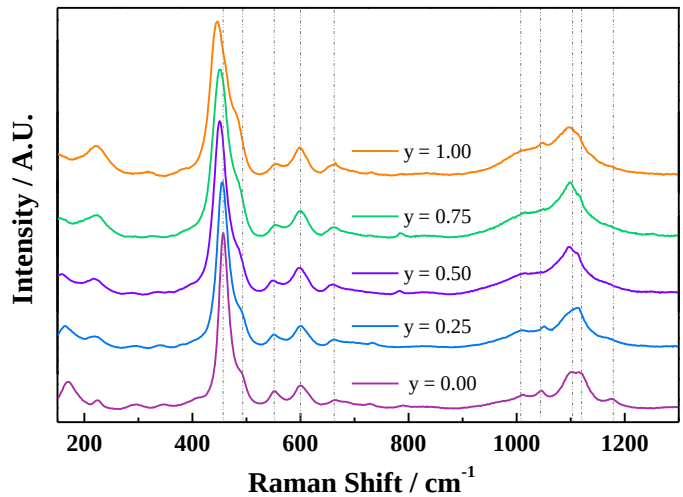

b)

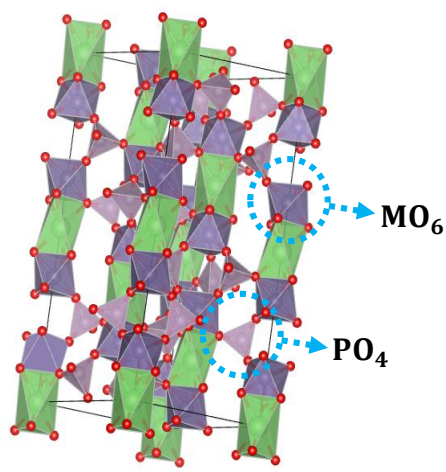

Figure 3.9 a) Raman spectrum of $Li_{1.5}Al_{0.5}Ge_{1.5-y}Sn_y(PO_4)_3$ in the frequency region of 150 to 1300 cm^{-1}. **b)** NASICON crystal structure where PO4 and MO6 structural groups are highlighted.

Figure 3.9a shows the Raman spectra of all the materials studied in this work and they were in good agreement with previous reports [12, 23]. Peaks in the range 300−500 cm^{-1} were attributed to components of ν_2 symmetric bending, while those in the range 500−800 cm^{-1} were components of ν_4 antisymmetric bending. The higher energy stretching modes were observed in the range 900−1300 cm^{-1} (ν_1, ν_3) [12, 23]. According to the literature, these last stretching modes ν_1 and ν_3 located in the frequency 850 – 1300 cm^{-1} are very sensitive to the PO_4 distortion and their peak broadening is an evidence[22]. For this reason, in Figure 3.10 it was amplified this range to study the local distortion of PO_4 as a function of Ge^{4+} substitution by Sn^{4+} in the system $Li_{1.5}Al_{0.5}Ge_{1.5-y}Sn_y(PO_4)_3$.

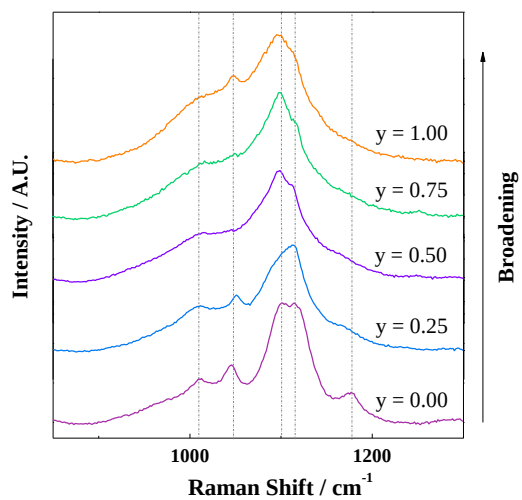

Figure 3.10 Raman spectra in the range of 850 – 1300 cm^{-1} for studying stretching modes ν_1 and ν_3.

Figure 3.10 shows the Raman spectra for the studied stretching modes. For y = 0.00 sample, the peaks agreed well with the literature [12]. Moreover, with the substitution of Ge^{4+} by Sn^{4+} it was observed slight peak broadening in all cases compared to y = 0.00 sample. This fact pointed out the existence of PO_4 distortion in the NASICON electrolytes containing Sn^{4+}.

3.5.1 Modification of the bottleneck regions as a function of PO_4 distortion

Al^{3+}, Ge^{4+} and Sn^{4+} are placed in the same site in the rhombohedral NASICON lattice. Analyzing the structure, it is reasonable to think that if MO_6 units containing Sn^{4+} are larger than MO_6 units containing Ge^{4+} or Al^{3+}, as a matter of fact, PO^4 units will need to rotate and/or distort to accommodate the size difference. Moreover, each oxygen is shared in a bond with $M^{4+/3+}$ cation, this points out an effect on the MO_6 units too as illustrated in Figure 3.11. The heavier M atoms may remain fairly ordered, and the MO_6 units respond to the lattice strain primarily through rotation about the c-axis. This rotation of MO_6 units will distort the geometry of the bottleneck by squeezing these regions for the further closure of the pathways and a trapping of Li^+ and finally decreasing the ionic conductivity as shown in Figure 3.8, but specially for samples with level of substitution y = 0.25 and y = 0.50[12].

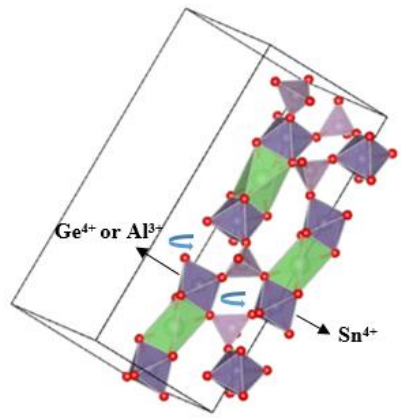

Figure 3.11 MO_6/PO_4 rotation and/or distortion.

3.6 Electronic conductivity

Figure 3.12a shows the normalized curves current vs. time of $Li_{1.5}Al_{0.5}Ge_{1.5-y}Sn_y(PO_4)_3$ according to the level of substitution. All samples showed current drop and further stabilization confirming that NASICON electrolytes were predominantly ionic conductors. Moreover, Figure 3.12b shows the calculated electronic conductivity vs. substitution level. For y = 0.00 sample the sample shown electronic conductivities in good agreement with previous reports[20, 24]. As long as tin was incorporated to the structure, the electronic conductivity decreased gradually compared to sample y = 0.00. And it showed a slightly increase for y = 1.00. This overall decrease in the electronic conductivity is beneficial for solid electrolytes in order to avoid self-discharge in the batteries.

a)

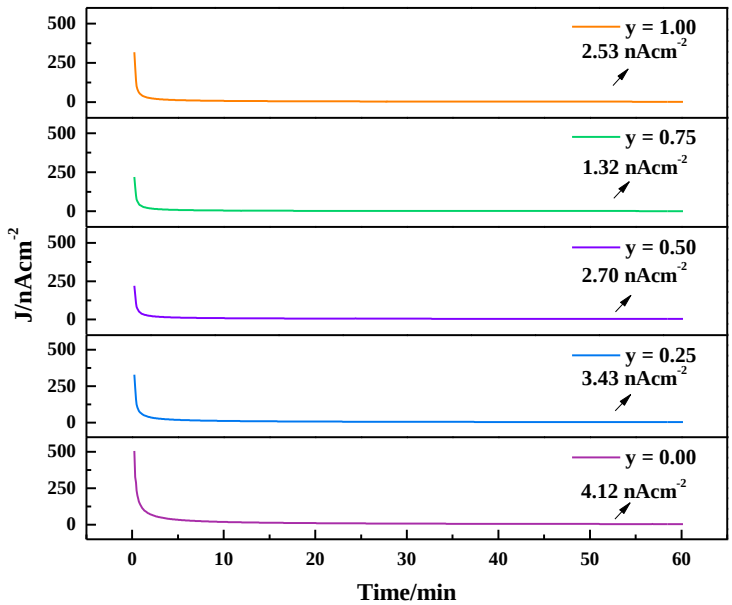

b)

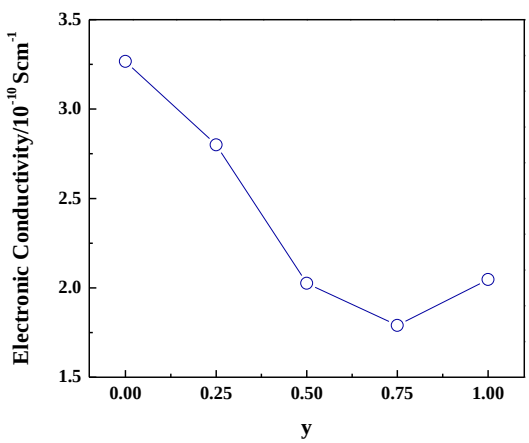

Figure 3.12 a) Experimental result of the electronic conductivity measurement vis DC-polarization method. **b)** Electronic conductivity as a function substitution condition of $Li_{1.5}Al_{0.5}Ge_{1.5-y}Sn_y(PO_4)_3$ at 25 °C.

Table 3.3 summarize the electrical conductivities as well the activation energies, ionic transference number and relative densities for all studied samples.

Table 3.3 Summary total ionic conductivities, electronic conductivities, activation energy, ionic transference number and relative density with composition $Li_{1.5}Al_{0.5}Ge_{1.5-y}Sn_y(PO_4)_3$.

Sample $Li_{1.5}Al_{0.5}Ge_{1.5-y}Sn_y(PO_4)_3$	Total Ionic Conductivity (10^{-5} Scm^{-1}) at 25 °C	Activation energy (eV) at 25°C	Electronic Conductivity (10^{-10} Scm^{-1}) at 25°C	Ionic Transference Number t_i	Relative Density (%)
y = 0.00	8.70	0.360	3.27	0.999996	90.05
y = 0.25	5.34	0.380	2.80	0.999995	85.56
y = 0.50	6.51	0.370	2.03	0.999997	92.33
y = 0.75	5.61	0.386	1.79	0.999997	91.90
y = 1.00	5.59	0.392	2.05	0.999996	88.91

Chapter 4. Conclusion

1) The influence of Sn inclusion on the conductivities of $Li_{1.5}Al_{0.5}Ge_{1.5-y}Sn_y(PO_4)_3$ was investigated.
2) Impedance studies confirmed that Sn^{4+} addition produced lower ionic conductivity at various concentration levels. However, all conductivity values were in the same order of magnitude.
3) The decrease in ionic conductivity was due to the local disorder in the MO_6 units group in the NASICON crystal structure which results in a distortion of the bottleneck regions reducing the charge carrier mobility. This was confirmed by Raman analysis.
4) The prepared materials had a lower electronic conductivity which is a desirable property for LIB in order to avoid self-discharge of the cells.
5) It was found three new materials in the system $Li_{1.5}Al_{0.5}Ge_{1.5-y}Sn_y(PO_4)_3$, among them $Li_{1.5}Al_{0.5}Ge_{0.50}Sn_{1.00}(PO_4)_3$ has the higher substitution level and ionic conductivity comparable to the well-known $Li_{1.5}Al_{0.5}Ge_{1.5}(PO_4)_3$, this expands more the research on inexpensive oxide solid electrolytes feasible for applications.

References

[1] G. Delaizir, N. Manafi, G. Jouan, P. Rozier, M. Dollé, All-solid-state silver batteries assembled by Spark Plasma Sintering, Solid State Ionics 207 (2012) 57-63.

[2] Y. Wang, W.D. Richards, S.P. Ong, L.J. Miara, J.C. Kim, Y. Mo, G. Ceder, Design principles for solid-state lithium superionic conductors, Nat Mater 14(10) (2015) 1026-31.

[3] H. Chung, B. Kang, Increase in grain boundary ionic conductivity of Li1.5Al0.5Ge1.5(PO4)3 by adding excess lithium, Solid State Ionics 263 (2014) 125-130.

[4] M. Pérez-Estébanez, J. Isasi-Marín, A. Rivera-Calzada, C. León, M. Nygren, Spark plasma versus conventional sintering in the electrical properties of Nasicon-type materials, Journal of Alloys and Compounds 651 (2015) 636-642.

[5] D.C.S. John T. S. Irvine, Anthony R. West, Electroceramics: Characterization by Impedance Spectroscopy, Advanced Materials 2 (1990) 132-138.

[6] R.C. Agrawal, dc Polarisation: An experimental tool in the study of ionic conductors, Indian Journal of Pure & Applied Physics 37 (1999) 294-301.

[7] Y.-C. Jung, M.-S. Park, C.-H. Doh, D.-W. Kim, Organic-inorganic hybrid solid electrolytes for solid-state lithium cells operating at room temperature, Electrochimica Acta 218 (2016) 271-277.

[8] H. Kitaura, H. Zhou, Reaction and degradation mechanism in all-solid-state lithium-air batteries, Chemical Communications 51(99) (2015) 17560-17563.

[9] Y. Zhu, Y. Zhang, L. Lu, Influence of crystallization temperature on ionic conductivity of lithium aluminum germanium phosphate glass-ceramic, Journal of Power Sources 290 (2015) 123-129.

[10] J.-M. Winand, A. Rulmont, P. Tarte, Nouvelles solutions solides LI(MIV)2−x(NIV)x(PO4)3 (L = Li,Na M,N = Ge,Sn,Ti,Zr,Hf) synthèse et étude par diffraction x et conductivité ionique, Journal of Solid State Chemistry 93(2) (1991) 341-349.

[11] S.H. Santagneli, H.V.A. Baldacim, S.J.L. Ribeiro, S. Kundu, A.C.M. Rodrigues, C. Doerenkamp, H. Eckert, Preparation, Structural Characterization, and Electrical Conductivity of Highly Ion-Conducting Glasses and Glass Ceramics in the System Li1+xAlxSnyGe2-(x+y)(PO4)3, The Journal of Physical Chemistry C 120(27) (2016) 14556-14567.

[12] B.E. Francisco, C.R. Stoldt, J.-C. M'Peko, Lithium-Ion Trapping from Local Structural Distortions in Sodium Super Ionic Conductor (NASICON) Electrolytes, Chemistry of Materials 26(16) (2014) 4741-4749.

[13] W.-J. Cui, J. Yi, L. Chen, C.-X. Wang, Y.-Y. Xia, Synthesis and electrochemical characteristics of NASICON-structured LiSn2(PO4)3 anode material for lithium-ion batteries, Journal of Power Sources 217 (2012) 77-84.

[14] X. Xu, Z. Wen, X. Wu, X. Yang, Z. Gu, Lithium Ion-Conducting Glass?Ceramics of Li1.5Al0.5Ge1.5(PO4)3?xLi2O (x=0.0?0.20) with Good Electrical and Electrochemical Properties, Journal of the American Ceramic Society 90(9) (2007) 2802-2806.

[15] V.A. Vizgalov, T. Nestler, L.A. Trusov, I.A. Bobrikov, O.I. Ivankov, M.V. Avdeev, M. Motylenko, E. Brendler, A. Vyalikh, D.C. Meyer, D.M. Itkis, Enhancing lithium-ion conductivity in NASICON glass-ceramics by adding yttria, CrystEngComm 20(10) (2018) 1375-1382.

[16] A. Kubanska, L. Castro, L. Tortet, O. Schäf, M. Dollé, R. Bouchet, Elaboration of controlled size Li1.5Al0.5Ge1.5(PO4)3 crystallites from glass-ceramics, Solid State Ionics 266 (2014) 44-50.

[17] S.S. Berbano, J. Guo, H. Guo, M.T. Lanagan, C.A. Randall, Cold sintering process of Li1.5Al0.5Ge1.5(PO4)3 solid electrolyte, Journal of the American Ceramic Society 100(5) (2017) 2123-2135.

[18] J. Yang, Z. Huang, B. Huang, J. Zhou, X. Xu, Influence of phosphorus sources on lithium ion conducting performance in the system of Li2O–Al2O3–GeO2–P2O5 glass–ceramics, Solid State Ionics 270 (2015) 61-65.

[19] H. El-Shinawi, A. Regoutz, D.J. Payne, E.J. Cussen, S.A. Corr, NASICON LiM2(PO4)3 electrolyte (M = Zr) and electrode (M = Ti) materials for all solid-state

Li-ion batteries with high total conductivity and low interfacial resistance, Journal of Materials Chemistry A 6(13) (2018) 5296-5303.

[20] M.R. Busche, T. Drossel, T. Leichtweiss, D.A. Weber, M. Falk, M. Schneider, M.L. Reich, H. Sommer, P. Adelhelm, J. Janek, Dynamic formation of a solid-liquid electrolyte interphase and its consequences for hybrid-battery concepts, Nat Chem 8(5) (2016) 426-34.

[21] P. Maldonadomanso, M. Martinsedeno, S. Bruque, J. Sanz, E. Losilla, Unexpected cationic distribution in tetrahedral/octahedral sites in nominal Li1+xAlxGe2−x(PO4)3 NASICON series, Solid State Ionics 178(1-2) (2007) 43-52.

[22] M. Barj, H. Perthuis, P. Colomban, Relations between sublattice disorder, phase transitions and conductivity in NASICON, Solid State Ionics 9-10 (1983) 845-850.

[23] P. Tarte, A. Rulmont, C. Merckaert-Ansay, Vibrational spectrum of nasicon-like, rhombohedral orthophosphates MIMIV2(PO4)3, Spectrochimica Acta Part A: Molecular Spectroscopy 42(9) (1986) 1009-1016.

[24] J.K. Feng, L. Lu, M.O. Lai, Lithium storage capability of lithium ion conductor Li1.5Al0.5Ge1.5(PO4)3, Journal of Alloys and Compounds 501(2) (2010) 255-258.

Acknowledgment

I can say it's been a nice journey this two years and a half in Korea with good moments but also with blue ones as everyone does.

At the end of this page, I would like to write down my SINCERE gratitude to my advisor Prof. Kwang Seon Shin. My life has been blessed with him from the very beginning because he gave me the chance to become a better professional in SNU. I gave me my best and hopefully, it was enough to correspond to the trust he put on me to carry out my research. After every GM, I always kept something from him for my research or life. Thank you, Prof. Shin~ Blessings, for your life and family~ I definitely will miss you.

I would like to give my SINCERE gratitude to Prof. Kisuk Kang too, for accepting to be my co-advisor and giving me the opportunity to carry out my research in his lab. I learned many things from his lectures during the semesters and from the individual meeting we had in his office.

I would like to thank Professor Yung-Eun Sung too. I took one lecture from him, however, this was enough to consider him a good professor. Thank you for asking me how I was doing with my research and for your guidelines.

I would like to also thank all my lab mates in MML. I don't want to give names because I considered to all of them really good friends. I really enjoyed their

friendship, jokes and I learned many things from them and without them, I couldn't be finishing my thesis. Will miss you guys forever.

In AEM Lab. I would like to thank Dr. Kyu-Yong Park. I consider to him a really good professional in the field of lithium batteries, but most importantly a really nice person. I am so thankful to him for his help, discussions, and support. I want to thank too to Myeong Hwan too, for making time to discuss my experiments and also for his friendship. Also to Orapa for being always willingness for helping me to book some equipment or things like downloading data, or having Thai food :) these things just showed me the quality of person she is. Thanks to Dr. Sung Joo Dr. JJ, SK, Hyunah, In-Sang, Hyeokjun, Kyungho, Donggun, Joo Ha and Do-hoon for the random short talks we had in AEM Lab. and even for things like helping me to print my ppt files at the last moment. I would have liked to share more time with guys to know you better.

Also, I would like to thank my home church "SNU International Church". My life in Korea changed dramatically in a positive way after I started to join them. In this place, I learned to love people no matter the differences in our outer shells. This place was wonderful and I really felt loved and support from them from the beginning. Will definitely miss to all of you SNUIC. Here I don't want to give names too since I consider all the members very important to my life.

All the things I experienced were blessings, but without my parents' support, I couldn't have had the opportunity to have an academic journey. Thank you Papi

Narcizo and Thank you mami Benita. I respect you and will take care of you since you showed me love working hard, to allow us to have better opportunities in our lives.

I want to thank my sponsors “Ministerio de Educacion” and “Yacimientos de Litio Boliviano” for trusting in me and given me financial support. My compromise is with Bolivia and once get back I will be helping with my grain of sand to the projects which can improve the quality of life of all Bolivian families.

In the end, I can’t just forget to Author of everything. Thank you, dear Lord, for being faithful and patient with me. Thank you for all the blessings you prepared for me in Korea. This chance to study at SNU made me understand that you are real and creator of all laws on earth.

Misael Ali Mita

2018 년 8 월